Anabolic actions of Notch on mature bone

Peng Liu[a,b,1,2], Yilin Ping[b,1], Meng Ma[c,1], Demao Zhang[b,1], Connie Liu[c], Samir Zaidi[d], Song Gao[e], Yaoting Ji[a,e], Feng Lou[b], Fanyuan Yu[b], Ping Lu[a], Agnes Stachnik[a], Mingru Bai[b], Chengguo Wei[c], Liaoran Zhang[b], Ke Wang[b], Rong Chen[c], Maria I. New[f,2], David W. Rowe[g], Tony Yuen[a], Li Sun[a,1], and Mone Zaidi[a,c,1,2]

[a]The Mount Sinai Bone Program, Department of Medicine, Mount Sinai School of Medicine, NY 10029; [b]State Key Laboratory of Oral Disease, West China School of Stomatology, Sichuan University, Sichuan 610041, China; [c]Department of Genetics and Genomic Sciences, Mount Sinai School of Medicine, NY 10029; [d]Department of Genetics, Yale School of Medicine, New Haven, CT 06520; [e]School of Stomatology, Wuhan University, Wuhan 430079, China; [f]Department of Pediatrics, Mount Sinai School of Medicine, NY 10029; and [g]Department of Reconstructive Sciences, School of Dental Medicine, University of Connecticut School of Medicine, Farmington, CT 06030

Contributed by Maria I. New, February 29, 2016 (sent for review December 10, 2015; reviewed by Di Chen, Christopher Huang, and Roberto Pacifici)

Notch controls skeletogenesis, but its role in the remodeling of adult bone remains conflicting. In mature mice, the skeleton can become osteopenic or osteosclerotic depending on the time point at which Notch is activated or inactivated. Using adult EGFP reporter mice, we find that Notch expression is localized to osteocytes embedded within bone matrix. Conditional activation of Notch signaling in osteocytes triggers profound bone formation, mainly due to increased mineralization, which rescues both age-associated and ovariectomy-induced bone loss and promotes bone healing following osteotomy. In parallel, mice rendered haploinsufficient in γ-secretase presenilin-1 (Psen1), which inhibits downstream Notch activation, display almost-absent terminal osteoblast differentiation. Consistent with this finding, pharmacologic or genetic disruption of Notch or its ligand Jagged1 inhibits mineralization. We suggest that stimulation of Notch signaling in osteocytes initiates a profound, therapeutically relevant, anabolic response.

osteoporosis | aging | therapeutic target | skeletal mineralization

Notch is a transmembrane receptor protein that upon ligand binding is cleaved by γ-secretases, including presenilin-1/2 (Psen1/2), to yield an active Notch intracellular domain (Nicd) that undergoes nuclear translocation (1). Within the nucleus, Nicd interacts with the DNA binding protein, recombination signal-binding protein for Ig κ J region (Rbpj), to regulate the expression of target genes. This canonical Notch signaling pathway includes the receptors Notch1–4, their ligands Jagged1/2 and Dll1-3, the primary nuclear binding protein Rbpj, and downstream genes, such as *Hes1/5* (2). Global deletion of any one or more of these genes renders mice embryonically lethal, likely due to deficiencies in somite maturation (3–9). Analysis of these embryos reveals defects in axial skeletal development, which is broadly recapitulated in descriptions of people harboring loss-of-function mutations in *Notch1/2* or *Dll3* (8, 10–12).

Though studies on the global deletion of Notch components have been difficult to interpret, there are seemingly conflicting reports on the skeletal phenotype of mice in which *Notch1/2* or *Psen1/2* is deleted, even in a cell-specific manner. Early deletion of *Notch1*, for example, using *Prx1-Cre* mice, causes postnatal lethality and radiodense bones (13). In contrast, late-stage *Notch1* deletion using a *Col2.3-Cre* line yields an osteoporotic phenotype (14). The effects of *Nicd* overexpression also yield opposing phenotypes depending upon the promoter used. Osteoporosis results when Nicd overexpression is driven by the *Col3.6* promoter (15), whereas mice are rendered severely osteosclerotic when either *Col2.3* or *Dmp1* promoters are used (16, 17).

Thus, it has been difficult to separate known early effects of Notch on skeletogenesis and postnatal modeling from potential therapeutically relevant effects on the mature skeleton, even in mutants that survive. In addition, gain-of-function studies have been fraught with interpretational dilemmas due to the apparent cell- and stage-specific function of Notch. Here, we show that cell-specific Notch induction in adult mice triggers a skeletal anabolic response. This bone-forming action, which we find is driven predominantly by increased mineralization, overcomes both age-related and ovariectomy-induced bone loss, and promotes bone healing in an osteotomy model; this prompts the potential for exploiting the Notch pathway to a therapeutic advantage.

Results

Notch Expression in Osteocytes and New Bone Formation. It is well recognized that Notch is critical for skeletogenesis (18–20), but its expression profile and physiological function in adult bone is not established. We therefore first sought to investigate the expression of activated Notch in trabecular and cortical bone of adult mice using a Notch reporter mouse, *cp-EGFP* [transgenic Notch reporter (TNR)]. TNR mice, initially developed for studying Notch expression in neural (21) and hematopoietic stem cells (22), respond to the intranuclear accumulation of Nicd upon activation. Thus, cellular fluorescence is noted only when Notch is activated.

Frozen sections of trabecular (femur metaphysis and spine), membranous (calvaria), or cortical (femur diaphysis) bone showed that cp-EGFP is localized to osteoblasts and osteocytes (Fig. 1 *A–D*). Notably, whereas cp-EGFP$^+$ osteocytes were embedded within the bone matrix (red arrow), surface cells were spindle-shaped, reminiscent of an osteoblast-to-osteocyte transition phenotype (white arrow). Single labeling with Xylenol orange of non-decalcified femur showed that cp-EGFP$^+$ cells lay in the vicinity of and, in fact, at points overlapped with sites of new bone formation (Fig. 1*A*). cp-EGFP$^+$ cells were not detected in a range of mouse tissues, including liver, spleen, lung, kidney, heart, vessel, muscle, and skin, with minimal expression noted in adult brain

Significance

Notch is a critical regulator of skeletal development, but its role in remodeling of the adult skeleton is unclear. Using genetically modified mice, we show that Notch stimulates skeletal mineralization by bone-building osteoblasts. Thus, overexpression of the Notch intracellular domain in mice results in an increase in bone mass, prevents bone loss following ovariectomy and during aging, and promotes fracture healing. Notch is therefore a potential therapeutic target for conditions of bone loss, including osteoporosis.

Author contributions: P. Liu, D.W.R., and M.Z. designed research; P. Liu, Y.P., M.M., D.Z., C.L., S.Z., S.G., Y.J., F.L., F.Y., P. Lu, A.S., M.B., C.W., L.Z., and K.W. performed research; P. Liu, Y.P., M.M., D.Z., C.L., S.Z., S.G., R.C., T.Y., L.S., and M.Z. analyzed data; and P. Liu, M.I.N., T.Y., L.S., and M.Z. wrote the paper.

Reviewers: D.C., Rush University; C.H., University of Cambridge; and R.P., Emory University School of Medicine.

Conflict of interest statement: M.Z. consults for Merck, Roche, Novartis, and a number of other companies, including Jeffries, Gerson Lehrman Group, and Guidepoint.

[1]P. Liu, Y.P., M.M., D.Z., L.S., and M.Z. contributed equally to this work.

[2]To whom correspondence may be addressed. Email: mone.zaidi@mssm.edu, liupossible@gmail.com, or maria.new@mssm.edu.

This article contains supporting information online at www.pnas.org/lookup/suppl/doi:10.1073/pnas.1603399113/-/DCSupplemental.

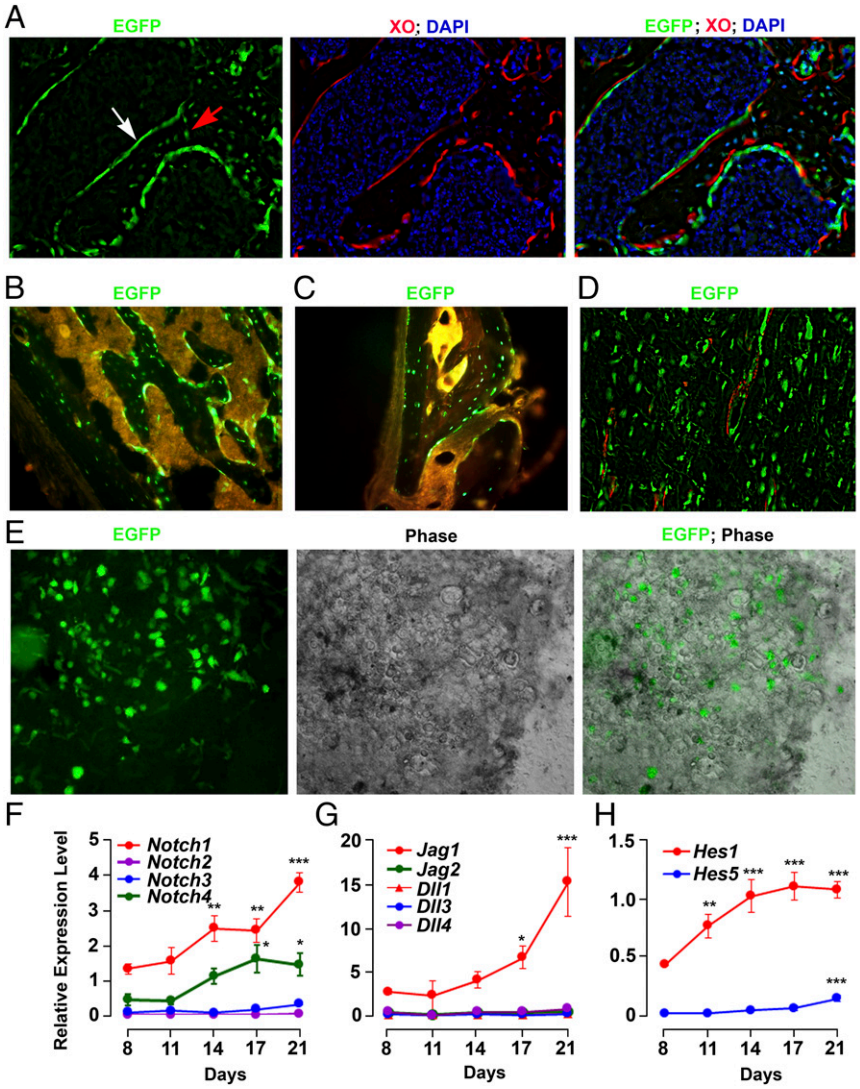

Fig. 1. Osteocytic expression of active Notch. Representative fluorescence micrographs showing EGFP expression (green) in trabecular [femur metaphysis (*A*) (40× magnification) and spine (*B*) (20× magnification)], membranous [calvarial sutures (*C*) (20× magnification)], and cortical [femur diaphysis (*D*) (40× magnification)] bone in adult, 2-mo-old *cp-EGFP* TNR mice. Red and blue staining, respectively, show Xylenol orange (XO) labeling, indicating areas of new bone formation, and DAPI staining of cell nuclei. Note the close proximity of EGFP expression and XO staining (*A*). $n = 6$ (male and female, aged 2–4 mo). (*E*) BMSC cultures (day 14–16; 20× magnification) from TNR mice ($n = 4$ per culture), showing $EGFP^+$ cells (*Left*, green) localized to mineralizing nodules (*Center*, black), with overlapping images shown (*Right*, triplicates/time point, five repeats). Expression (quantitative PCR) of *Notch1-4* (*F*), the ligands *Jagged1/2* (*Jag1/2*) and *Dll1/3/4* (*G*), and downstream target genes, *Hes1/5* (*H*) in BMSC cultures from *C57BL/6J* mice, as a function of days in differentiating medium. $n = 5$, triplicates per time points. $^{***}P < 0.001$, $^{**}P < 0.01$, $^{*}P < 0.05$, compared with day 8 (one-way ANOVA with Bonferroni post hoc test). All experiments were performed at least two times.

(Fig. S1). This finding suggests physiologically specific localization of Notch signaling to bone and brain.

We sought further to explore the temporal expression of activated Notch as a function of osteoblast differentiation in bone marrow stromal cell cultures (BMSCs). cp-$EGFP^+$ cells were not detected during early osteoblast differentiation (days 4 and 7) by fluorescent microscopy. However, strongly $EGFP^+$ cells resembling osteocytes were found embedded in mineralized areas at ∼day 10 of culture (Fig. S2). After day 16, upon the completion of mineralization, active cp-$EGFP^+$ cells were lost. This narrow window of Notch activity in adult bone specifically points to its putative role in regulating mineralization.

The presence of active Notch in vivo would require the presence not only of the Notch receptor, but also of ligand and target gene(s). We therefore examined the expression (quantitative PCR) in bone marrow cultures of the *Notch1–4*, the Notch ligands *Jag1/2* and *Dll1/3/4*, and the downstream target genes *Hes1/5*. *Notch1* and *4* showed a progressive increase in expression over time (Fig. 1*F*). Increasing expression was also noted for *Jag1* and *Hes1*, but not for *Jag2*, *Dll1/3/4*, or *Hes5* (Fig. 1 *G* and *H*). These results are consistent with a function of Notch in the mineralization of adult bone.

Notch Signaling Is Required for Mineralization. To determine whether Notch signaling is required for mineralization, we used four complementary approaches. We first examined mineralization by isolated BMSCs in the presence of a γ-secretase inhibitor DAPT (*N*-[*N*-(3,5-difluorophenacetyl)-L-alanyl]-S-phenylglycine t-butyl ester); the latter is known to block Notch endoproteolysis. Cells were cultured in the presence of β-glycerolphosphate and stained for cfu-fibroblastoid (cfu-f; alkaline phosphatase labeled) at day 10, or cfu-osteoblastoid (cfu-ob; von Kossa labeled) at days

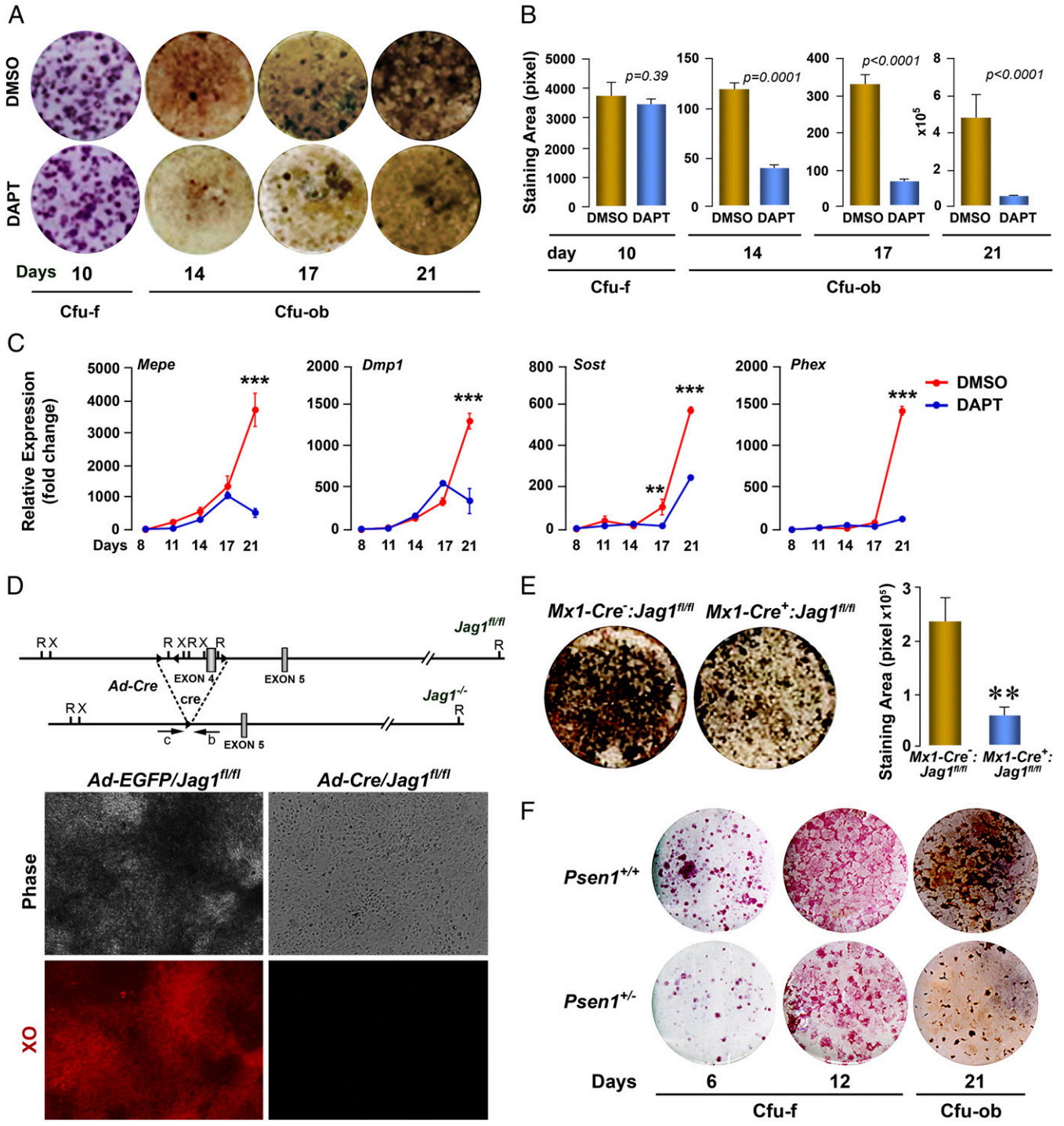

Fig. 2. Pharmacologic and genetic evidence for a role for Notch in mineralization. Representative images (*A*) and colony area (*B*) showing the effect of the γ-secretase inhibitor DAPT (or DMSO, vehicle) on alkaline phosphatase-labeled cfu-f or von Kossa-labeled cfu-ob in BMSC cultures undergoing differentiation. RNA extracted from BMSC cultures treated with DAPT or DMSO underwent quantitative PCR for markers of osteocytes and mineralization, including *Mepe*, *Dmp1*, *Sost*, and *Phex*. Statistics: unpaired Student's *t* test, comparisons between DAPT and DMSO; *P* values shown (*B*), $n = 3$ wells per group; in quadruplicate (*C*). (*D*) Dramatic reduction of mineralization [phase contrast images, *Upper*; Xylenol orange (XO) labeling, *Lower*] when BMSC cultures from $Jag1^{fl/fl}$ mice were infected with *Ad-Cre* to delete exon 4 of the *Jag1* gene under differentiating conditions. $n = 3$ wells/group in quadruplicate. (*E*) Similarly dramatic reduction in von Kossa-labeled cfu-ob colonies in cultures from $Mx1\text{-}Cre^{+}\text{:}Jag1^{fl/fl}$ mice, shown both as representative plates and as staining area. $n = 3$ wells per group, in quadruplicate. (*F*) Profound reduction in cfu-ob with modest decrements in early cfu-f colonies in BMSCs from *Psen1* haploinsufficient ($Psen1^{+/-}$) mice. $n = 3$ wells per group. $^{***}P < 0.0001$, $^{**}P < 0.001$, compared with day 8 (one-way ANOVA with Sidak's correction for multiple comparisons). All experiments were performed at least two times.

14, 17, and 21. DAPT strongly inhibited cfu-ob, but not cfu-f formation, consistent with a late effect of Notch signaling inhibition on mineralization (Fig. 2 *A* and *B*); this was associated with markedly reduced expression of mineralization-associated genes—namely, *matrix extracellular phosphoglycoprotein* (*Mepe*), *dentin matrix protein-1* (*Dmp1*), *sclerostin* (*Sost*), and *phosphate*

regulating endopeptidase homolog X-linked (*Phex*). Importantly, gene expression at earlier time points remained unaffected (Fig. 2*C*).

Second, we studied the mineralizing activity of BMSCs in which the Notch ligand, *Jag1,* was conditionally deleted using *Ad-Cre*. A profound reduction in mineralization was visualized using phase contrast microscopy and by Xylenol orange staining (Fig. 2*D*). In a third set of experiments, we cultured BMSCs isolated from mice in which *Jag1* was deleted conditionally in cells of the hematopoietic and mesenchymal lineages using an *Mx1-Cre* promoter and polyI:polyC. Again, a gross reduction in mineralization was noted on von Kossa staining (Fig. 2*E*). Finally, we cultured bone marrow stromal cells from mice haploinsufficient for *Psen1* (23). Expectedly, there was a profound reduction in cfu-ob formation; however, there was also an unexplained decrease in cfu-f, likely arising from alternative actions of *Psen1* (Fig. 2*F*). These

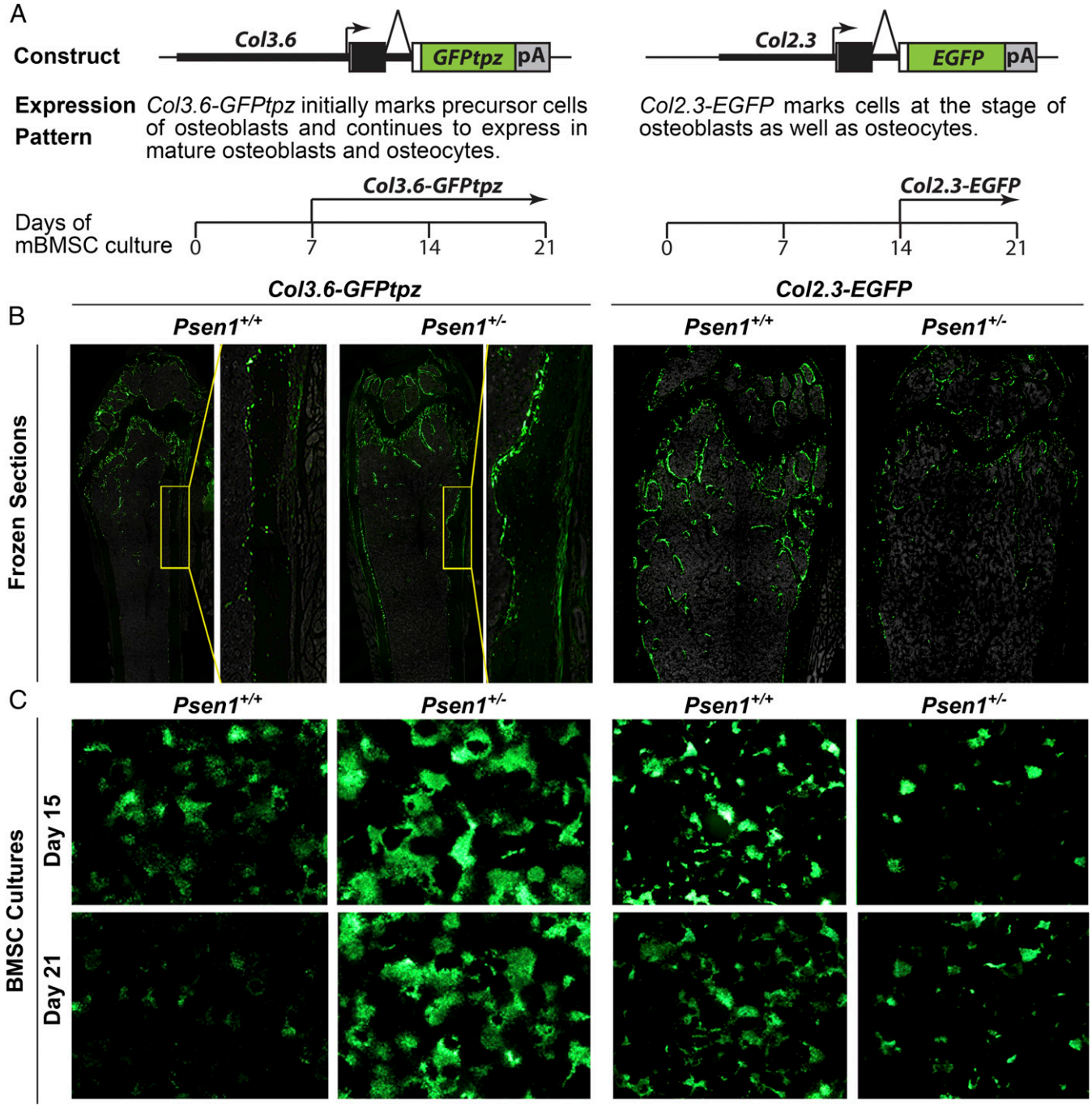

Fig. 3. Lineage tracing osteoblasts in *Psen1* haploinsufficient mice reveals a block in differentiation. A schematic representation of expression patterns for *Col3.6-GFPtpz* and *Col2.3-EGFP* (*A*). Tracking EGFP^{+} osteoblasts in *Col3.6-GFPtpz* (early expression) or *Col2.3-EGFP* (late expression) mice on a wild-type or *Psen1*$^{+/-}$ background, both in vivo in the cortical and trabecular compartments of the femur (*B*) (female, *Col3.6-GFPtpz* aged 3 mo and *Col2.3-EGFP* aged 6 mo), as well as in vitro in BMSC cultures (*C*). Representative frozen sections and wells are shown: (*B*) 20× magnification; box showing magnified area 40×; (*C*) 20× magnification (n = 3–5 per group, aged 2–4 mo). All experiments were performed at least three times.

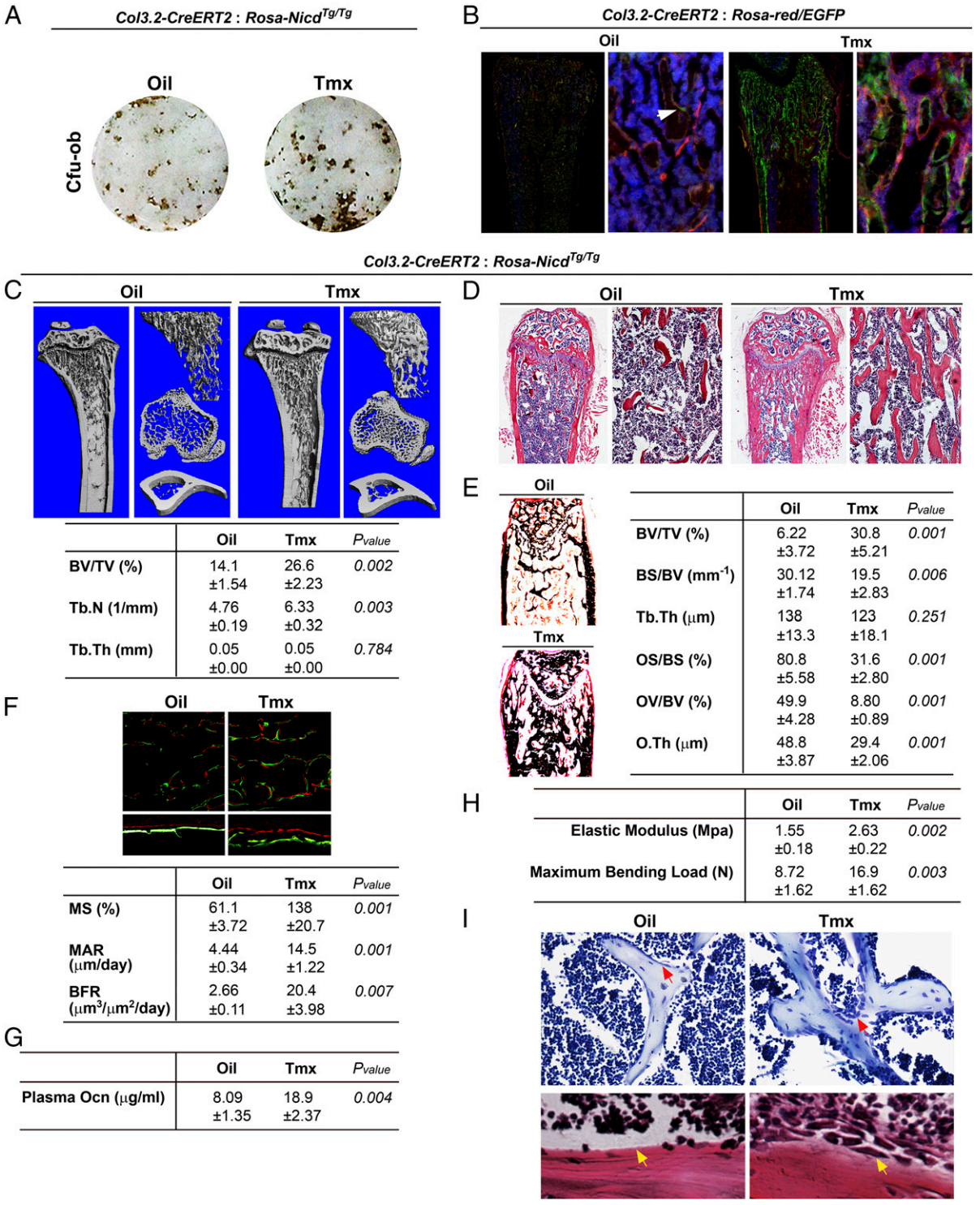

	Oil	Tmx	P_{value}
BV/TV (%)	14.1 ±1.54	26.6 ±2.23	0.002
Tb.N (1/mm)	4.76 ±0.19	6.33 ±0.32	0.003
Tb.Th (mm)	0.05 ±0.00	0.05 ±0.00	0.784

	Oil	Tmx	P_{value}
BV/TV (%)	6.22 ±3.72	30.8 ±5.21	0.001
BS/BV (mm^{-1})	30.12 ±1.74	19.5 ±2.83	0.006
Tb.Th (μm)	138 ±13.3	123 ±18.1	0.251
OS/BS (%)	80.8 ±5.58	31.6 ±2.80	0.001
OV/BV (%)	49.9 ±4.28	8.80 ±0.89	0.001
O.Th (μm)	48.8 ±3.87	29.4 ±2.06	0.001

	Oil	Tmx	P_{value}
MS (%)	61.1 ±3.72	138 ±20.7	0.001
MAR (μm/day)	4.44 ±0.34	14.5 ±1.22	0.001
BFR ($\mu m^3/\mu m^2$/day)	2.66 ±0.11	20.4 ±3.98	0.007

	Oil	Tmx	P_{value}
Plasma Ocn (μg/ml)	8.09 ±1.35	18.9 ±2.37	0.004

	Oil	Tmx	P_{value}
Elastic Modulus (Mpa)	1.55 ±0.18	2.63 ±0.22	0.002
Maximum Bending Load (N)	8.72 ±1.62	16.9 ±1.62	0.003

Fig. 4. Conditional activation of Notch in osteoblasts of adult mice induces new bone formation. (*A*) Representative plates showing increased von Kossa-labeled mineralization in response to Tmx treatment of BMSC cultures from *Col3.2-CreERT2:Rosa-Nicd*$^{Tg/Tg}$ mice (n = 4 triplicate wells per group). (*B*) Fluorescence micrographs of frozen section of femur from reporter *Col3.2-CreERT2:Rosa-red/EGFP* mice to demonstrate EGFP expression in response to Cre activation by Tmx (*Left*, 5× magnification; *Right*, 20×). Note that mice treated with vehicle (oil) show minimal EGFP leakage (white arrow, also see Fig. S5*A*) (n = 3–6 per group, male, aged 2–3 mo). Effects of Notch activation by Tmx in 16-wk-old *Col3.2-CreERT2:Rosa-Nicd*$^{Tg/Tg}$ mice. The femur (trabecular and cortical bone) was evaluated by μCT (*C*), H&E staining (*D*, 5× and 20× magnification), or von Kossa labeling (*E*, 5× magnification). Note the substantial increase in bone mass. Microstructural parameters include bone volume/total volume (BV/TV), trabecular number (Tb.N), trabecular thickness (Tb.Th), osteoid surface/bone surface (OS/BS), osteoid volume/bone volume (OV/BV), and osteoid thickness (O.Th). Shown also are plasma osteocalcin levels (*G*). Dynamic histomorphometry in calcein/Xylenol orange dual-labeled mice displaying the dramatic effect of Notch induction on mineralizing surface (MS), MAR, and BFR (*F*) (units as shown). Representative images are also shown. Measures of bone strength, including elastic modulus and maximum bending load, on a three-point bending test, are shown (*H*). (*I*) Toluidine blue and H&E staining of femoral metaphysis and cortex, respectively, showing osteoblasts (arrows, 40× magnification). Unpaired Student's t test, comparisons between oil- and Tmx-treated mice; P values shown, n = 5 mice per group, male. Results are expressed as mean ± SEM.

data together confirm that the activation of Notch is a requirement for mineral deposition.

To explain the cellular basis for the reduced mineralization in *Psen1*$^{+/-}$ mice, we tracked cells of the osteoblast lineage using reporter mice that expressed GFP during early and late osteoblast progression. We crossed *Psen1*$^{+/-}$ mice with *Col3.6-GFPtpz* or *Col2.3-EGFP* mice (24), respectively, and lineage tracked GFP^{+} cells in adult mice in vivo, as well as ex vivo in BMSC cultures at 15 and 21 d. Previous studies with *Col3.6-GFPtpz* mice have shown that the *3.6 kb Col1a1* promoter is extensively expressed, in addition to skin, in osteoblasts lining the periosteal and endosteal trabecular surfaces, with weak expression in periosteal spindle-shaped preosteoblasts (24). In contrast, the 2.3-kb *Col1a1* promoter marks mature osteoblasts and osteocytes in *Col2.3EGFP* mice (24). In differentiating bone marrow stromal cell cultures, GFP expression is seen as early as days 7 and 14, respectively, for *Col3.6-GFPtpz* and *Col2.3EGFP* mice (24) (Fig. 3*A*).

We found a notable abundance of GFP^{+} cells in frozen sections (Fig. 3*B*) and BMSC cultures (Fig. 3*C*) from *Col3.6-GFPtpz*:*Psen1*$^{+/-}$ mice compared with *Col3.6-GFPtpz*:*Psen1*$^{+/+}$ littermates. However, there was a marked reduction in GFP^{+} cells in *Col2.3-EGFP*:*Psen1*$^{+/-}$ mice compared with *Col2.3-EGFP*:*Psen1*$^{+/+}$ mice (Fig. 3 *B* and *C*). This suggests that haploinsufficiency of *Psen1*, a surrogate for Notch signaling, blocked lineage progression to mature mineralizing osteoblasts.

Controlled Notch Overexpression in Osteoblast Lineage Cells Stimulates Bone Formation. To test the direct effects of Notch activation on bone formation and bone mass, we characterized the skeletons of mice overexpressing Nicd specifically in cells of the osteoblast lineage. Because Notch is expressed in osteocytes (Fig. 1), we initially crossed *Dmp1-Cre* mice with *Rosa-Nicd*$^{Tg/Tg}$ mice (25). Nicd overexpression in *Dmp1-Cre*$^{+}$:*Rosa-Nicd*$^{Tg/Tg}$ mice led to postnatal death at ∼20 d. H&E staining of femur epiphyseal sections showed significantly increased bone volume, with infiltration and ablation of the bone marrow cavities (Fig. S3). To circumvent osteosclerosis resulting from the noninducible, persistent expression of Nicd by *Dmp1-Cre*, we selected *Col3.2-CreERT2* to achieve a spatiotemporal control of Nicd activity in mature osteoblasts and osteocytes in bone, as previously reported (26–29). Of note is that the expression of the 3.2-kb *Col1a1* promoter is restricted to mature osteoblasts and osteocytes similarly to the 2.3-kb *Col1a1* promoter, but is distinct from that of the *Col3.6* promoter. Notably, the 3.2-kb promoter is not active in spindle-shaped periosteal preosteoblasts, where the 3.6-kb promoter is predominantly expressed (24). As such, our premise is that expression of *Nicd* using the inducible 3.2-kb promoter will closely mimic any effects driven by the 2.3-kb promoter (26, 29).

In separate experiments, we found that *Ad-Cre*-mediated Nicd overexpression in BMSCs caused a profound increase in mineralization (Fig. S4). The direct effect of Nicd activity on mineralization was confirmed in tamoxifen-induced BMSCs from *Col3.2-CreERT2:Rosa-Nicd*$^{Tg/Tg}$ mice (Fig. 4*A*). Using *Col3.2-CreERT2*:*Rosa-red/EGFP* reporter mice, we confirmed tamoxifen-induced EGFP expression selectively and efficiently in osteocytes and osteoblasts (Fig. 4*B*); its expression pattern is known to be similar to that of *Col2.3-EGFP* and is different from *Col3.6-GFPtpz*, notably without detectable EGFP expression in periosteal preosteoblasts (24). However, low levels of EGFP expression were noted in noninduced, corn oil-treated mice (Fig. S5*A*). Microstructural bone and osteoid parameters on μCT or von Kossa staining remained unaffected despite the leaky EGFP expression (Fig. S5 *B* and *C*), thus validating noninduced, corn oil-treated *Col3.2-CreERT2*:*Rosa-Nicd*$^{Tg/Tg}$ mice as controls.

μCT of trabecular and cortical bone from adult homozygotic *Col3.2-CreERT2*:*Rosa-Nicd*$^{Tg/Tg}$ showed a dramatic increase in bone mass. There was a significant increase in bone volume/total volume (BV/TV) and trabecular number (Tb.N) in tamoxifen-induced mice compared with corn oil-treated controls (Fig. 4*C*). H&E staining showed marked increases in trabecular bone with infiltration of bone marrow (Fig. 4*D*). Von Kossa staining further showed not only increases in BV/TV, but also reduced osteoid parameters, including osteoid surface/bone surface (OS/BS), osteoid volume/bone volume (OV/BV), and osteoid thickness (O.Th), consistent with increased mineralization (Fig. 4*E*). Dynamic histomorphometry showed profound increases in mineral apposition rate (MAR) and bone formation rate (BFR; Fig. 4*F*), indicative of overall increases in bone formation. The enhanced bone formation, confirmed by increased serum osteocalcin levels (Fig. 4*G*), together with disproportionately high hypermineralization, likely resulted in markedly improved bone strength—namely, elastic modulus and maximum bending on a three-point bending test (Fig. 4*H*). Overall, therefore, selective activation of Notch signaling in mature osteoblasts and osteocytes stimulates new bone synthesis and increases bone strength. An almost-identical phenotype was evident in heterozygotic *Col3.2-CreERT2:Rosa-Nicd*$^{Tg/+}$ mice (Fig. S6).

At the cellular level, we examined osteoblast and osteoclast numbers through toluidine blue and tartrate-resistant acid phosphatase (Trap) staining, respectively. Osteoblast numbers were expectedly increased in *Col3.2-CreERT2*:*Rosa-Nicd*$^{Tg/Tg}$ mice (Fig. 4*I*). There was also an increase in parameters of bone resorption, including Oc.N/BS and Oc.S/BS, as well as serum Trap5b levels, likely arising from retained osteoblast–osteoclast coupling (Fig. S7 *A* and *B*). This increase in bone resorption is consistent with an increase in osteoclast formation in response to low subnanomolar concentrations of *Jag1* added to BMSCs. Osteoclast formation was inhibited at higher nanomolar concentrations (Fig. S7*C*).

Biologically Relevant Effects of Notch Signaling in Osteocytes. To establish Notch as a viable target for the modulation of adult bone remodeling, we injected recombinant *Jag1* directly onto calvaria of 3-mo-old adult C57BL/6J mice. There was a profound anabolic effect, with a significant increase in new bone formation assessed in H&E stain (Fig. 5*A*).

To complement a skeletal anabolic response genetically in relevant biological models, we examined the effects of Nicd overexpression in aging and ovariectomized mice, as well as in an osteotomy model. Induction of Nicd by tamoxifen in *Col3.2-CreERT2:Rosa-Nicd*$^{Tg/+}$ mice at 8 mo of age, at which time bone mass is known to be reduced, resulted in osteoprotection. Notably, μCT of spinal trabecular bone showed marked increases in BV/TV and Tb.N, with a corresponding decrease in Tb.Sp (Fig. 5*B*). Von Kossa staining of femur metaphyseal (trabecular) bone not only confirmed an increase in BV/TV, but also showed diminished OV/BV and O.Th, consistent with increased mineralization (Fig. 5*C*); this was accompanied by an overall increase in bone formation parameters—namely, mineralizing surface (MS) and BFR (Fig. 5*D*). Additionally, there was dramatic thickening of the cortical component of the femur (Fig. 5*C*).

In separate experiments, 3-mo-old *Col3.2-CreERT2*:*Rosa-Nicd*$^{Tg/Tg}$ mice were ovariectomized and immediately injected with either corn oil or tamoxifen. Expectedly, there was a dramatic loss of bone in corn oil-treated control mice 8 wk following surgery (Fig. 5*E*). However, there was an obvious and significant increase in BV/TV and Tb.Th in tamoxifen-induced mice (Fig. 5*E*), which was accompanied by a dramatic reduction in osteoid parameters, confirming that Notch signaling protected against bone loss following ovariectomy.

Finally, we assessed the effect of Notch activation in adult mice on fracture healing using a femur osteotomy model. For this, a 3-mm defect was created surgically, 3 d after which the mice were given corn oil or tamoxifen for 4 wk. Plain radiography [In-Vivo Xtreme (Bruker)] showed that there was complete restoration of the

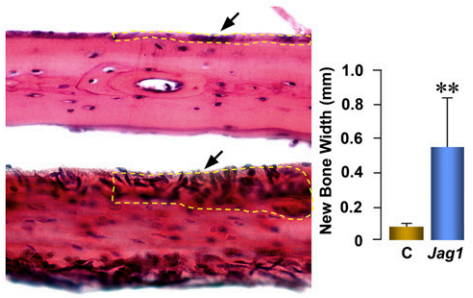

B 8 Month-old *Col3.2-CreERT2:Rosa-Nicd*$^{Tg/+}$ Mice

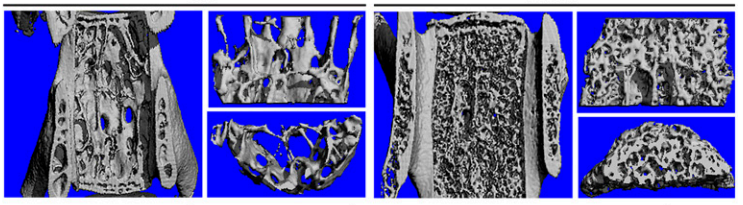

	Oil	Tmx	*P*value
BV/TV (%)	19.3 ±2.85	33.0 ±5.49	*0.014*
Tb.N (1/mm)	4.51 ±0.36	7.71 ±0.94	*0.018*
Tb.Th (μm)	0.05 ±0.00	0.05 ±0.00	*0.369*
Tb.Sp (μm)	0.23 ±0.02	0.14 ±0.02	*0.012*

C 8 Month-old *Col3.2-CreERT2:Rosa-Nicd*$^{Tg/+}$ Mice

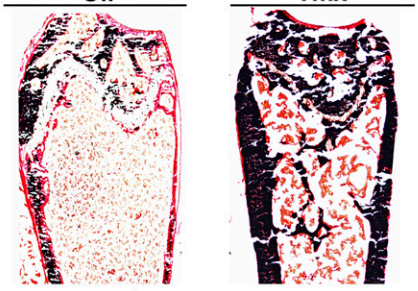

	Oil	Tmx	*P*value
BV/TV (%)	14.6 ±4.73	71.0 ±18.9	*0.031*
BS/BV (mm^{-1})	64.8 ±14.3	29.4 ±5.02	*0.036*
Tb.Th (μm)	132 ±53.4	113 ±14.6	*0.347*
OS/BS (%)	56.7 ±15.0	71.9 ±5.07	*0.214*
OV/BV (%)	64.3 ±8.32	34.6 ±2.86	*0.029*
O.Th (μm)	64.8 ±7.97	41.7 ±4.37	*0.012*
Ct.Th (μm)	13.9 ±3.68	39.1 ±3.51	*<0.001*

D

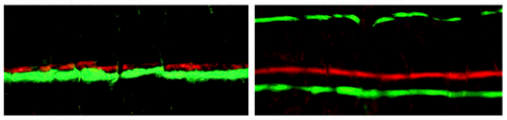

Trabecular	Oil	Tmx	*P*value
MS (%)	7.06 ±0.81	17.8 ±2.41	*0.005*
MAR (μm/day)	1.05 ±0.23	1.29 ±0.13	*0.389*
BFR ($\mu m^3/\mu m^2$/day)	0.08 ±0.03	0.23 ±0.05	*0.031*

E Ovariectomized *Col3.2-CreERT2:Rosa-Nicd*$^{Tg/+}$ Mice

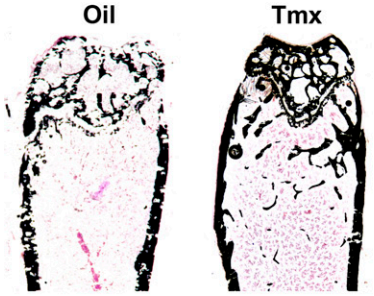

	Oil	Tmx	*P* value
BV/TV (%)	1.43 ±0.38	5.78 ±2.12	*0.003*
BS/BV (%)	37.1 ±5.82	22.7 ±3.51	*0.003*
Tb.Th (μm)	59.7 ±9.70	90.03 ±14.8	*0.007*
OS/BS (%)	8.04 ±4.25	0.16 ±0.05	*0.008*
OV/BV (%)	4.02 ±1.42	0.08 ±0.01	*0.001*

F

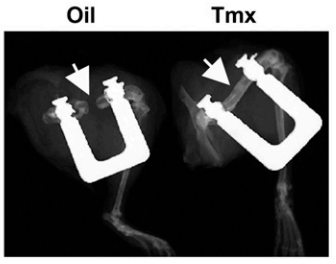

Fig. 5. Conditional Notch activation in adult mice rescues bone loss and promotes bone healing. (*A*) Anabolic action of recombinant Jag1 injected onto calvarial bone of adult mice (40 μg/kg, 20× magnification), $n = 5$ per group, male B6, aged 2 mo. Evaluation of spine by μCT (*B*) and femur metaphysis by von Kossa staining (*C*, 5× magnification) following the induction of Notch expression in 8-mo-old *Col3.2-CreERT2:Rosa-Nicd*$^{Tg/+}$ mice by Tmx injections. Microstructural parameters as in Fig. 4. (*D*) Complementary dynamic histomorphometry of calcein/XO dual-labeled mice displaying the effect of Notch induction on MS, MAR, and BFR (units as shown). Representative images are also shown (40× magnification). (*E*) Von Kossa staining (5× magnification) and microstructural parameters, including osteoid parameters, of femur metaphysis following Tmx injection in ovariectomized *Col3.2-CreERT2:Rosa-Nicd*$^{Tg/Tg}$ mice. Unpaired Student's *t* test, comparisons between oil- and Tmx-treated mice; *P* values shown (*B*), $n = 4$–5 mice/group. (*F*) Plain radiograph (In-Vivo Xtreme) showing the effect Notch activation by Tmx on the healing of an osteotomy defect induced in femur diaphysis, $n = 5$ per group.

surgical defect in tamoxifen-induced *Col3.2-CreERT2*:*Rosa-Nicd*$^{Tg/Tg}$ mice, whereas mice receiving oil continued to display nonunion (Fig. 5*F*).

Discussion

We report the effects of active Notch signaling on adult bone. Hitherto, Notch has been considered a key developmental gene that coordinates a variety of transcriptional events to regulate somitogenesis and stem cell fate (30–36). In the skeletal context, studies have focused primarily on bone development in both mice and people. Mutations of Notch components are known to cause defects in axial skeletal development. For example, spondylocostal dysostosis results from mutations in human *DLL3* (10, 11, 37, 38), a Notch ligand, whereas *NOTCH2* mutations alone cause Hagdu–Cheney syndrome, a rare disease characterized by facial abnormalities, acro-osteolysis and, interestingly, osteoporosis (39, 40). Mutations of *JAG1* and *NOTCH2* in concert cause Alagille syndrome, marked by impaired craniofacial development due to somite segmentation defects.

However, mice lacking individual Notch receptors are invariably lethal in utero, likely due to an early deficiency in somite segmentation (7, 9–11, 41–47). Nonetheless, double-mutant mice, wherein *Prx1-Cre*-mediated deletion of *Psen1* is restricted to the mesenchyme on a *Psen2*$^{-/-}$ background, survive for up to 10 wk and display radiodense bones (13). This phenotype is recapitulated in mice in which both *Notch1* and *Notch2* are deleted from the early mesenchyme, again using *Prx1-Cre* (13). However, deletion of *Psen1* solely in osteoblast-lineage cells using a *Col2.3-Cre* line yields an osteoporotic phenotype (14). The opposing skeletal phenotypes of mice in which Notch components are deleted using *Prx1*- or *Col2.3-Cre* lines suggests that Notch effects are cell specific and dependent on the stage of development.

Gain-of-function studies also yield opposing phenotypes depending on promoter used to drive Notch overexpression. Mice transgenically expressing Nicd under Col2.3 or Dmp1 promoters, which allow restricted expression in osteoblast-lineage cells and osteocytes, respectively, display osteosclerosis with bone marrow infiltration at 4 wk followed by early postnatal death (17). These findings support the possibility that Notch signaling has an anabolic action on adult bone. In contrast, early osteoblast lineage overexpression of Nicd using *Col3.6-Cre* mice suppresses progression of the osteoblast to a more mature, mineralizing phenotype, yielding an osteopenic phenotype (15, 48). These conflicting phenotypes seem to arise from both cell- and stage-dependence of Notch effects, and call for a definitive phenotypic characterization of mice in which Nicd is overexpressed solely during adulthood.

Because *Col3.6-Cre* is noninducible, and expressed in bone, teeth, and other nonbone tissues, such as skin, brain, kidney, liver, and lung (24, 49), we used *Col3.2-CreER* in which Cre is inducible and expressed in a similar pattern to *Col2.3-Cre* (24)—namely, its expression is limited in bone and teeth with a lower expression in tendon, but without detection of GFP expression in other tissues, such as skin, brain, kidney, liver, and lung) (26, 29). Within bone, *Col3.6* is expressed in precursor cells in the suture mesenchyme, as well as in preosteoblasts and the fibrous layers of the inner and outer periosteum and their downstream progeny (24). In contrast, *Col2.3* and *Col3.2* are identified specifically in osteoblasts and osteocytes (26–29). We surmise that the reported osteoporotic phenotype of *Col3.6-Cre*:*Rosa-Nicd*$^{Tg/Tg}$ may be caused by early and constant Nicd activation that likely interrupts physiological lineage transition from the preosteoblast into mature osteoblasts and osteocytes (15). In addition, *Col3.6-GFP* has been reported to be expressed in osteoclasts (50), making it further difficult to interpret outcomes. In contrast, we report that *Col3.2-CreERT*:*Rosa-Nicd*$^{Tg/Tg}$ mice that are induced to overexpress Nicd in osteoblast lineage cells during adulthood display a dramatic anabolic bone phenotype. Arising from increased osteoblastic bone formation, prominently as a result of advanced mineralization, this anabolic phenotype overcomes age-associated osteopenia and prevents postovariectomy-induced bone loss. These latter studies suggest that Notch, if targeted during adult life, could offer potential opportunities for new therapies. To this end, we further show that induction of Nicd in osteoblast lineage cells can result in the rapid healing of surgical defects in an osteotomy model.

Another issue unresolved from previous studies relates to the cell type that Notch primarily regulates in adult bone. We find that the actions of Notch in osteoblast lineage cells are primarily osteocyte driven. Several findings underscore this premise. First, our analysis of *Notch-EGFP* reporter mice documents EGFP^{+} cells within bone matrix; osteocytes are the only cells known to be embedded in bone. Second, mice in which Nicd is overexpressed using the *Dmp1* promoter, known to be relatively specific for osteocytes, demonstrate profound osteosclerosis and postnatal lethality. Third, the osteocyte-mediated function of Notch is consistent with the predominant mineralization defect noted as reduced von Kossa staining and osteocytic gene expression in DAPT-treated BMSC cultures and absent mineralization in cultures in which *Jag1* is deleted in vitro using *Ad-Cre* or ex vivo in *Mx1-Cre*$^{+}$:*Jag1*$^{fl/fl}$ mice. Fourth, by lineage tracing using two GFP reporter mice, we provide direct evidence that *Psen1* haploinsufficiency almost completely blocks the transition of osteoblast precursors to a more mature, mineralizing phenotype, with the consequent accumulation of precursor cells. This latter finding also explains osteoporotic phenotype of *Psen1*/*2*-deficient mice noted by others (13, 51). With that said, we are by no means excluding other actions of Notch signaling during earlier stages of osteoblast development, although we believe that the predominant effects occur late during mineralization.

Our complementary approaches that collectively demonstrate direct anabolic effects of Notch on adult bone raise the question of whether Notch or its components are drug-able targets for osteoporosis. More than 100 million men and women suffer from osteoporosis worldwide, and many of these patients have low-turnover bone loss that could be best treated by an anabolic agent (52). Nonetheless, the armamentarium of anabolic therapies is restricted to just recombinant human parathyroid hormone. Targeting the osteocyte toward an anabolic response may provide a viable alternative, which could be achieved either by stimulating the Wnt pathway, an approach that is currently underway (53–56), or, as we suggest, by stimulating Notch signaling.

However, the extent to which any bone-forming therapy would have a net positive effect on bone mass in people would depend on whether it also stimulates bone resorption to counter its anabolic action. We find that, despite the stimulation of osteoclastic bone resorption, Notch overexpression, at least in mice, yields a profound net anabolic phenotype, which is in contrast to the stimulation of Wnt signaling, wherein the anabolic action of an anti-sclerostin antibody is paralleled by an inhibition, rather than stimulation, of bone resorption (20, 56–58). Though this finding may suggest that Wnt stimulation may be efficacious with a greater net effect on bone mass, a key advantage of targeting Notch over the Wnt pathway resides in the relative selectivity of its expression in bone, with limited expression in the adult brain. Wnt, however, is significantly more ubiquitously distributed and has a role in oncogenesis (59). Therefore, expression of Notch in the brain may necessitate a fuller evaluation, because mutations in presenilins and γ-secretases are known to predispose to Alzheimer's disease.

Methods

Mice. All mouse experiments were performed per approved protocols by the Institutional Animal Care and Use Committees at Sichuan University and Icahn Medical School at Mount Sinai. Three mouse lines were purchased from JAX, including the TNR line [*Tg*(*Cp-EGFP*)*25*Gaia/ReyaJ; 018322]; conditional Nicd transgenic line [*Gt*(*ROSA*)*26Sortm1*(*Notch1*)Dam/J; 008159]; *Rosa-ACTB-tdTomato,-EGFP* [*Gt*(*ROSA*)*26Sor*$^{tm4(ACTB-tdTomato,-EGFP)Luo}$/J; 007576]; and

Mx1-Cre transgenic lines [*Tg*(*Mx1-Cre*)*1*Cgn/J; 003556]. The *Col3.6-GFPtpz* and *Col2.3-EGFP* lines were obtained from D.W.R.'s laboratory (24). *Col3.2-CreERT2* mice were kindly provided by Jerry Feng, Texas A&M University, Dallas and Henry M. Kronenberg, Harvard University, Boston (27). The 3.6-kb collagen 1a1 proximal promoter (*Col3.6*) is active during early osteoblast differentiation, whereas the shorter 2.3-kb and 3.2-kb promoters (*Col2.3* and *Col3.2*) are active during late osteoblast differentiation. *Jag1*$^{flox/flox}$ [*B6;129S-Jag1*^{tm2Grid}/J; 010618] and Notch transgenic mice [*C57BL/6J-Tg*(*ACTB-NOTCH1*)*1*Shn/J; 006481] mice were kindly supplied by Thomas Gridley (JAX). *Psen1* mutant mice were provided by Jorge Busciglio (60). For conditional Notch activation, male *Col3.2-CreERT2* mice were crossed with female transgenic mice (either *Rosa-Nicd* or *Rosa-ACTB-tdTomato,-EGFP*). Tamoxifen (Tmx; Sigma-Aldrich; catalog no. 10540-29-1) was injected at a dose of 75 mg/kg, once a day for 6 or 10 d, respectively, into mature (8- to 10-wk-old) or aged (8-mo-old) mice, as described previously (61, 62). Littermate controls were injected with corn oil (vehicle). The mice were killed 2 wk after injection. Each group consisted of five or six mice.

Mouse Bone Marrow Stromal Cell Culture. Primary BMSCs were performed using bone marrow from mouse femurs and tibia as previously described (63). Briefly, bone marrow was flushed from femora and tibia and cultured in α-modified Eagle's MEM (Life Technologies) supplemented with 10% (vol/vol) FBS (HyClone Laboratories) and 1% penicillin/streptomycin (Life Technologies) at a cell density of $\sim 20 \times 10^6$/mL. For osteogenic differentiation, cells were maintained in basal medium for 7 d, and then changed to osteogenic medium (supplemented with 10^{-8} M dexamethasone, 8 mM β-glycerophosphate, and 50 μg/mL ascorbic acid) for 14 d. Alkaline phosphatase (Alp)-positive colonies (or cfu-f) and von Kossa-labeled mineralizing colonies (or cfu-ob), respectively, were counted 7 and 21 d after culture. ImageJ software v1.41a (NIH) was used to determine areas of Alp and von Kossa staining. *Ad-Cre* and *Ad-EGFP* were obtained from Yingzi Yang (NIH).

Osteoclast cultures were performed as described previously (64). Briefly, bone marrow hematopoietic cells were plated in the presence of macrophage colony-stimulating factor (MCSF) (30 ng/ml) for 2 d, followed with both MCSF and receptor activator of nuclear factor kappa-B ligand (Rankl) (25 ng/ml) for 3–5 d. Osteoclast cultures were fixed in 3.7% (vol/vol) formaldehyde and 0.1% Triton X-100 for 5 min, and stained for Trap. Trap$^+$ cells with more than two nuclei were counted as osteoclasts.

Histology and Bone Histomorphometry. Decalcified and nondecalcified sections of bone were obtained, as described previously (65). Briefly, mice were injected s.c. with calcein (10 mg/kg; Sigma) 8 d (adult mice) or 12 d (aging mice), after which they received a Xylenol orange (90 mg/kg; Sigma) injection. Lumbar vertebrae (L1–4) were fixed with 4% (vol/vol) paraformaldehyde for 18 h at 4 °C. Nondecalcified bones were embedded in optimum cutting temperature compound (O.C.T. compound, Tissue-Tek), and 5- to 7-μm-thick frozen sections were prepared using a transparent film. Static and dynamic histomorphometric analyses were performed according to standard protocols using software kindly provided by Robert J. van't Hof.

ELISA Assay. Mouse plasma was stored at −80 °C. ELISA kits were purchased for tartrate-resistant acid phosphatase 5b (Trap5b) and osteocalcin assays and used per manufacturer's protocol (catalog nos. SEA902Mu and SEA471Mu; Cloud Clone Corp.).

Microtomography. High-resolution μCT scanning (μCT50; Scanco) was performed to measure morphological indices of metaphyseal regions of femur or lumbar vertebrae (L5–6) as previously described (66). The bones were dissected, cleaned, fixed in 10% formalin, transferred to 75% (vol/vol) ethanol, loaded into 10-mm diameter scanning tubes, and imaged. Imaging analysis of metaphyseal regions was performed using 100 slices (10 μm/slice). The most proximal slice was defined as the plane where the growth plate had just disappeared. A Gaussian filter (σ, 0.8; support, 1) was applied to all analyzed scans. Key parameters were as follows: X-ray tube potential, 55 kVp; X-ray intensity, 145 μA; integration time, 200 ms; and threshold, 220 mg/cm^3.

Gene Expression Analysis. Total RNA was extracted with TRIzol reagent (Invitrogen) per manufacturer's protocol (67). RNA was treated with DNase and first-strand cDNA was synthesized using oligo(dT) primer and SuperScript II reverse transcriptase (Invitrogen). Quantitative real-time PCR was performed in triplicate by using iQ SYBR Green Supermix on a iCycler Real-Time Detection System (BioRad). The relative amount of mRNA was normalized by cyclophilin A expression.

Local Calvarial Injection of Recombinant Jagged1. Recombinant Jag1 protein was purchased from Sino Biological Inc. (catalog no. 11648-H02H) and injected onto the right side of the calvaria of adult mice using a technique described previously (68–70). Briefly, 8-wk-old C57BL/6J mice were injected with vehicle alone or Jag1 (40 μg/kg, once daily, for 6 d, 50 μL). On day 16, calvariae were harvested, fixed, and subjected to H&E staining, followed by measurement of new bone width.

Mechanical Testing. Three-point bending and compression/traction of long bones (femurs and tibias) were performed as described previously (71) using a mechanical testing device (Twin Column Table Mounted Testing System; Instron 5565).

Femur Osteotomy. Mouse femur osteotomy was performed in *Col3.2-CreERT2*:*Rosa-Nicd*$^{Tg/Tg}$ male mice previously reported (72) with modification. Briefly, general anesthesia was induced by i.p. injections of ketamine hydrochloride (750 mg/kg body weight) and xylazine (25 mg/kg body weight). The intramuscular septum between the vastus lateralis and the hamstring muscles was divided by blunt dissection to localize the femur. An external fixation device was attached to the right femur. Then, a 3-mm defect was created in the femur at the midshaft by means of a transverse osteotomy with a dental saw. Absorbable sutures were used to close the intramuscular septum and skin incision. Mice were randomized into each group. At 3 d postoperation, Tmx was injected i.p. every other day for 10 d ($n = 5$), and mice were killed 3 wk after the last injection. Corn oil was used as control ($n = 5$). Radiographs were obtained using an Optical In-Vivo Xtreme Imaging System (Bruker).

ACKNOWLEDGMENTS. We thank Drs. Jian Q. (Jerry) Feng and Henry M. Kronenberg for providing *Col3.2-CreERT2* and *Dmp1-Cre* mice; Drs. Mary L. Bouxsein and Brian C. Dawson for help with μCT protocols; Dr. Rob van't Hof for providing a bone histomorphometry software; Dr. Jorge Busciglio for *Psen1*$^{+/-}$ mice; Dr. Thomas Gridley for *Jag1*$^{fl/fl}$ and *Actb-Notch1*^{Tg} mice; Dr. Xi Jiang and Ms. Li Chen for assistance with frozen sections and fluorescence imaging; Dr. Liping Wang for assistance with the mouse osteotomy model; and Dr. Yingzi Yang for providing *Ad-Cre*. Support for this work was provided by National Science Foundation of China Grant 81070689 (to P. Liu); NIH Grants AG40132, AG23176, AR65932, and AR67066 (to M.Z.); and start-up funding from the National Key Lab of Oral Diseases, West China School of Stomatology, Sichuan University, China (P. Liu).

1. Artavanis-Tsakonas S, Muskavitch MA (2010) Notch: The past, the present, and the future. *Curr Top Dev Biol* 92:1–29.
2. Bray S, Bernard F (2010) Notch targets and their regulation. *Curr Top Dev Biol* 92: 253–275.
3. Jiang R, et al. (1998) Defects in limb, craniofacial, and thymic development in Jagged2 mutant mice. *Genes Dev* 12(7):1046–1057.
4. Kadokawa Y, Marunouchi T (2002) Chimeric analysis of Notch2 function: A role for Notch2 in the development of the roof plate of the mouse brain. *Dev Dyn* 225(2):126–134.
5. Hamada Y, et al. (1999) Mutation in ankyrin repeats of the mouse Notch2 gene induces early embryonic lethality. *Development* 126(15):3415–3424.
6. Huppert SS, et al. (2000) Embryonic lethality in mice homozygous for a processing-deficient allele of Notch1. *Nature* 405(6789):966–970.
7. Donoviel DB, et al. (1999) Mice lacking both presenilin genes exhibit early embryonic patterning defects. *Genes Dev* 13(21):2801–2810.
8. Xue Y, et al. (1999) Embryonic lethality and vascular defects in mice lacking the Notch ligand Jagged1. *Hum Mol Genet* 8(5):723–730.
9. Koizumi K, et al. (2001) The role of presenilin 1 during somite segmentation. *Development* 128(8):1391–1402.
10. Chapman G, Sparrow DB, Kremmer E, Dunwoodie SL (2011) Notch inhibition by the ligand DELTA-LIKE 3 defines the mechanism of abnormal vertebral segmentation in spondylocostal dysostosis. *Hum Mol Genet* 20(5):905–916.
11. Dunwoodie SL, et al. (2002) Axial skeletal defects caused by mutation in the spondylocostal dysplasia/pudgy gene Dll3 are associated with disruption of the segmentation clock within the presomitic mesoderm. *Development* 129(7):1795–1806.
12. Heath V (2011) Genetics: New data on Hajdu-Cheney syndrome turns up bone research a NOTCH. *Nat Rev Endocrinol* 7(6):311.
13. Hilton MJ, et al. (2008) Notch signaling maintains bone marrow mesenchymal progenitors by suppressing osteoblast differentiation. *Nat Med* 14(3):306–314.
14. Engin F, et al. (2008) Dimorphic effects of Notch signaling in bone homeostasis. *Nat Med* 14(3):299–305.
15. Zanotti S, et al. (2008) Notch inhibits osteoblast differentiation and causes osteopenia. *Endocrinology* 149(8):3890–3899.
16. Tao J, et al. (2010) Osteosclerosis owing to Notch gain of function is solely Rbpj-dependent. *J Bone Miner Res* 25(10):2175–2183.
17. Canalis E, et al. (2013) Notch signaling in osteocytes differentially regulates cancellous and cortical bone remodeling. *J Biol Chem* 288(35):25614–25625.

18. Regan J, Long F (2013) Notch signaling and bone remodeling. *Curr Osteoporos Rep* 11(2):126–129.
19. Engin F, Lee B (2010) NOTCHing the bone: Insights into multi-functionality. *Bone* 46(2):274–280.
20. Canalis E (2008) Notch signaling in osteoblasts. *Sci Signal* 1(17):pe17.
21. Mizutani K, Yoon K, Dang L, Tokunaga A, Gaiano N (2007) Differential Notch signalling distinguishes neural stem cells from intermediate progenitors. *Nature* 449(7160): 351–355.
22. Duncan AW, et al. (2005) Integration of Notch and Wnt signaling in hematopoietic stem cell maintenance. *Nat Immunol* 6(3):314–322.
23. Shen J, et al. (1997) Skeletal and CNS defects in Presenilin-1-deficient mice. *Cell* 89(4): 629–639.
24. Kalajzic I, et al. (2002) Use of type I collagen green fluorescent protein transgenes to identify subpopulations of cells at different stages of the osteoblast lineage. *J Bone Miner Res* 17(1):15–25.
25. Lu Y, et al. (2007) DMP1-targeted Cre expression in odontoblasts and osteocytes. *J Dent Res* 86(4):320–325.
26. Kamiya N, et al. (2008) Disruption of BMP signaling in osteoblasts through type IA receptor (BMPRIA) increases bone mass. *J Bone Miner Res* 23(12):2007–2017.
27. Maes C, et al. (2010) Osteoblast precursors, but not mature osteoblasts, move into developing and fractured bones along with invading blood vessels. *Dev Cell* 19(2): 329–344.
28. Rossert J, Terraz C, Dupont S (2000) Regulation of type I collagen genes expression. *Nephrol Dial Transplant* 15(Suppl 6):66–68.
29. Rossert J, Eberspaecher H, de Crombrugghe B (1995) Separate cis-acting DNA elements of the mouse pro-alpha 1(I) collagen promoter direct expression of reporter genes to different type I collagen-producing cells in transgenic mice. *J Cell Biol* 129(5): 1421–1432.
30. Liu J, Sato C, Cerletti M, Wagers A (2010) Notch signaling in the regulation of stem cell self-renewal and differentiation. *Curr Top Dev Biol* 92:367–409.
31. Ohishi K, Varnum-Finney B, Bernstein ID (2002) The notch pathway: Modulation of cell fate decisions in hematopoiesis. *Int J Hematol* 75(5):449–459.
32. Gaiano N, Fishell G (2002) The role of notch in promoting glial and neural stem cell fates. *Annu Rev Neurosci* 25:471–490.
33. Allman D, Punt JA, Izon DJ, Aster JC, Pear WS (2002) An invitation to T and more: Notch signaling in lymphopoiesis. *Cell* 109(Suppl):S1–S11.
34. Watt FM (2002) The stem cell compartment in human interfollicular epidermis. *J Dermatol Sci* 28(3):173–180.
35. Milner LA, Bigas A (1999) Notch as a mediator of cell fate determination in hematopoiesis: Evidence and speculation. *Blood* 93(8):2431–2448.
36. Sancho R, Cremona CA, Behrens A (2015) Stem cell and progenitor fate in the mammalian intestine: Notch and lateral inhibition in homeostasis and disease. *EMBO Rep* 16(5):571–581.
37. Beine O, et al. (2004) [Spondylocostal dysostosis: A rare genetic disease]. *Rev Med Liege* 59(9):513–516.
38. Bulman MP, et al. (2000) Mutations in the human delta homologue, DLL3, cause axial skeletal defects in spondylocostal dysostosis. *Nat Genet* 24(4):438–441.
39. Zhao W, et al. (2013) Mutations in NOTCH2 in patients with Hajdu-Cheney syndrome. *Osteoporos Int* 24(8):2275–2281.
40. Simpson MA, et al. (2011) Mutations in NOTCH2 cause Hajdu-Cheney syndrome, a disorder of severe and progressive bone loss. *Nat Genet* 43(4):303–305.
41. Wong PC, et al. (1997) Presenilin 1 is required for Notch1 and DII1 expression in the paraxial mesoderm. *Nature* 387(6630):288–292.
42. Kim W, et al. (2011) The period of the somite segmentation clock is sensitive to Notch activity. *Mol Biol Cell* 22(18):3541–3549.
43. Ferjentsik Z, et al. (2009) Notch is a critical component of the mouse somitogenesis oscillator and is essential for the formation of the somites. *PLoS Genet* 5(9):e1000662.
44. Dequéant ML, et al. (2006) A complex oscillating network of signaling genes underlies the mouse segmentation clock. *Science* 314(5805):1595–1598.
45. Gridley T (2006) The long and short of it: Somite formation in mice. *Dev Dyn* 235(9): 2330–2336.
46. Zhang N, Norton CR, Gridley T (2002) Segmentation defects of Notch pathway mutants and absence of a synergistic phenotype in lunatic fringe/radical fringe double mutant mice. *Genesis* 33(1):21–28.
47. Conlon RA, Reaume AG, Rossant J (1995) Notch1 is required for the coordinate segmentation of somites. *Development* 121(5):1533–1545.
48. Deregowski V, Gazzerro E, Priest L, Rydziel S, Canalis E (2006) Notch 1 overexpression inhibits osteoblastogenesis by suppressing Wnt/beta-catenin but not bone morphogenetic protein signaling. *J Biol Chem* 281(10):6203–6210.
49. Dacic S, Kalajzic I, Visnjic D, Lichtler AC, Rowe DW (2001) Col1a1-driven transgenic markers of osteoblast lineage progression. *J Bone Miner Res* 16(7):1228–1236.
50. Boban I, et al. (2006) The 3.6 kb DNA fragment from the rat Col1a1 gene promoter drives the expression of genes in both osteoblast and osteoclast lineage cells. *Bone* 39(6):1302–1312.
51. Dishowitz MI, Terkhorn SP, Bostic SA, Hankenson KD (2012) Notch signaling components are upregulated during both endochondral and intramembranous bone regeneration. *J Orthop Res* 30(2):296–303.
52. Zaidi M (2007) Skeletal remodeling in health and disease. *Nat Med* 13(7):791–801.
53. Canalis E (2013) Wnt signalling in osteoporosis: Mechanisms and novel therapeutic approaches. *Nat Rev Endocrinol* 9(10):575–583.
54. Gong Y, et al.; Osteoporosis-Pseudoglioma Syndrome Collaborative Group (2001) LDL receptor-related protein 5 (LRP5) affects bone accrual and eye development. *Cell* 107(4):513–523.
55. Li X, et al. (2010) Inhibition of sclerostin by monoclonal antibody increases bone formation, bone mass, and bone strength in aged male rats. *J Bone Miner Res* 25(12): 2647–2656.
56. McClung MR, et al. (2014) Romosozumab in postmenopausal women with low bone mineral density. *N Engl J Med* 370(5):412–420.
57. Zanotti S, Canalis E (2014) Notch1 and Notch2 expression in osteoblast precursors regulates femoral microarchitecture. *Bone* 62:22–28.
58. Padhi D, Jang G, Stouch B, Fang L, Posvar E (2011) Single-dose, placebo-controlled, randomized study of AMG 785, a sclerostin monoclonal antibody. *J Bone Miner Res* 26(1):19–26.
59. Janssens N, Janicot M, Perera T (2006) The Wnt-dependent signaling pathways as target in oncology drug discovery. *Invest New Drugs* 24(4):263–280.
60. Pigino G, Pelsman A, Mori H, Busciglio J (2001) Presenilin-1 mutations reduce cytoskeletal association, deregulate neurite growth, and potentiate neuronal dystrophy and tau phosphorylation. *J Neurosci* 21(3):834–842.
61. Breunig JJ, Silbereis J, Vaccarino FM, Sestan N, Rakic P (2007) Notch regulates cell fate and dendrite morphology of newborn neurons in the postnatal dentate gyrus. *Proc Natl Acad Sci USA* 104(51):20558–20563.
62. Anastassiadis K, Glaser S, Kranz A, Berhardt K, Stewart AF (2010) A practical summary of site-specific recombination, conditional mutagenesis, and tamoxifen induction of CreERT2. *Methods Enzymol* 477:109–123.
63. Sun L, et al. (2006) FSH directly regulates bone mass. *Cell* 125(2):247–260.
64. Colaianni G, et al. (2012) Bone marrow oxytocin mediates the anabolic action of estrogen on the skeleton. *J Biol Chem* 287(34):29159–29167.
65. Jiang X, et al. (2005) Histological analysis of GFP expression in murine bone. *J Histochem Cytochem* 53(5):593–602.
66. Bouxsein ML, et al. (2010) Guidelines for assessment of bone microstructure in rodents using micro-computed tomography. *J Bone Miner Res* 25(7):1468–1486.
67. Yuen T, Wurmbach E, Pfeffer RL, Ebersole BJ, Sealfon SC (2002) Accuracy and calibration of commercial oligonucleotide and custom cDNA microarrays. *Nucleic Acids Res* 30(10):e48.
68. Mundy G, et al. (1999) Stimulation of bone formation in vitro and in rodents by statins. *Science* 286(5446):1946–1949.
69. Garrett IR, et al. (2003) Selective inhibitors of the osteoblast proteasome stimulate bone formation in vivo and in vitro. *J Clin Invest* 111(11):1771–1782.
70. van 't Hof RJ, Clarkin CE, Armour KJ (2003) Studies of local bone remodeling. The calvarial injection assay. *Methods Mol Med* 80:345–351.
71. Volkman SK, et al. (2003) Quantitative trait loci for femoral size and shape in a genetically heterogeneous mouse population. *J Bone Miner Res* 18(8):1497–1505.
72. Zwingenberger S, et al. (2013) Establishment of a femoral critical-size bone defect model in immunodeficient mice. *J Surg Res* 181(1):e7–e14.